PCCP

ROYAL SOCIETY OF CHEMISTRY

Role of the conformational flexibility of evodiamine in its binding to protein hosts: A comparative spectroscopic and molecular modeling evaluation with rutaecarpine

SCHOLARONE™
Manuscripts

Manifestations of the structural flexibility of evodiamine
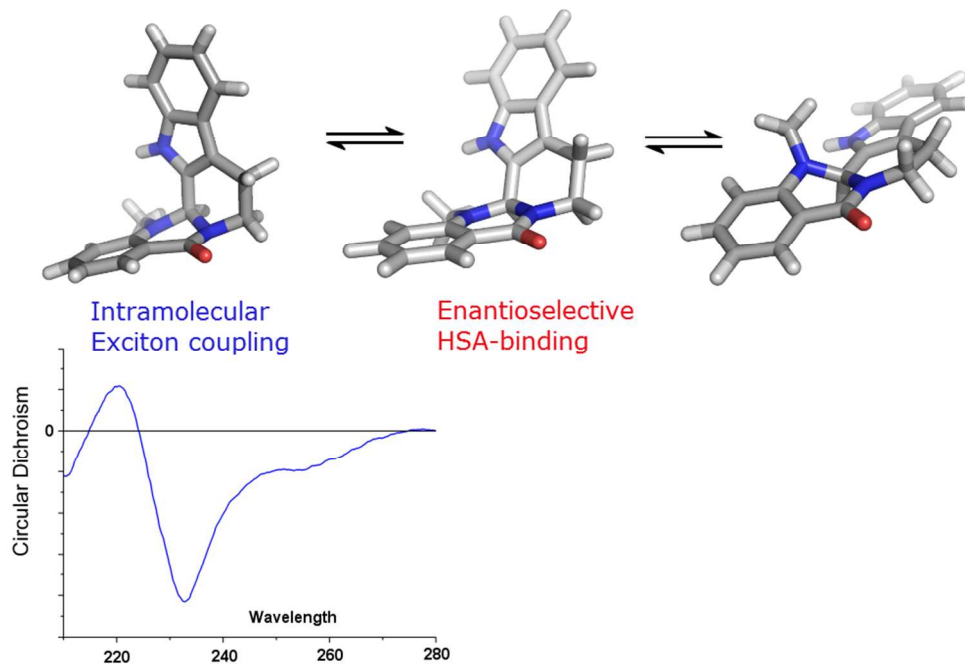
Inherent structural flexibility of evodiamine allows to adopt different conformations depending on the nature of the environment.

361x270mm (72 x 72 DPI)

Role of the conformational flexibility of evodiamine in its binding to protein hosts: A comparative spectroscopic and molecular modeling evaluation with rutaecarpine

Celesztina Domonkos, Ilona Fitos, Júlia Visy, Ferenc Zsila[*]

Research Group of Chemical Biology, Institute of Organic Chemistry,

Research Centre for Natural Sciences, Hungarian Academy of Sciences, POB 289,

H-1519, Budapest, Hungary

Corresponding author: Ferenc Zsila

POB 289, H-1519, Budapest, Hungary

Fax: (+36) 1-438-1145

Email: zsila.ferenc@ttk.mta.hu

Abstract

Spectroscopic studies combined with computational analysis indicate the inherent conformational flexibility of the β-carbolin derivative evodiamine (EVD) featured with diverse pharmacological activities. Qualitative evaluation of the circular dichroism (CD) spectra of EVD enantiomers complemented with quantum chemical calculations reveal a chiral exciton signature that can be assigned to the folded, L-shaped conformation of the molecule. Changes of the exciton couplet measured in different solvents and the near-UV CD profile upon binding to human serum albumin (HSA) refer to the structural adaptability of EVD. The enantioselectivity of EVD-HSA interaction is shown indicating the binding preference of the (*R*)-enantiomer. Comparison of experimental and calculated CD spectra of various conformers of EVD as well as the results of molecular docking data suggest that the (*R*)-antipode is accomodated within the subdomain IIA of HSA in ridge-tile conformation. Rutaecarpine (RTC), the close congener of EVD forms much tighter association complexes both with HSA and α_1-acid glycoprotein. In contrast to EVD, the nearly planar geometry of the indoloquinazoline ring system of RTC allows its stacked dimeric binding to HSA.

Introduction

The Evodiae fructus (*Evodiae rutaecarpa*, Rutaceae) known as "Wu Zhu Yu" in China and "Goshuyu" in Japan is one of the most popular multi-purpose herbal drug in East Asia. In traditional Chinese medicine, it has been utilized for hundreds of years for the treatment of gastrointestinal disorders, headache, amenorrhea and postpartum haemorrhage. Its pharmacological action and therapeutic efficiency is mainly related to the presence of two indoloquinazoline alkaloids (Scheme 1), evodiamine (EVD) and rutaecarpine (RTC).[1] These compounds exhibit various biological and pharmacological activities including vasodilatory, antinociceptive, thermoregulatory, cardiotonic, antithrombotic, analgesic, antiobesity, and uterotonic effects.[2] In addition, several reports have proved the anticancer and apoptotic activity of EVD on colon, lung, breast, prostate and hepatoblastoma cell lines.[3]

In this work, the stereochemical properties of EVD in relation to RTC were evaluted revealing its inherent conformational adaptability to distinct macromolecular hosts such as human serum albumin (HSA) and α_1-acid glycoprotein (AAG). Since EVD is a chiral molecule with an asymmetric centre at the C3 position, its binding stereoselectivity was elucidated, too. Enantiomers were obtained by resolution of the racemate using a recently developed method.[4] The applied techniques included circular dichroism (CD), UV and fluorescence spectroscopy, molecular modeling, affinity chromatography on HSA-Sepharose column, and chiral HPLC. In addition, the experimental CD spectra were compared with calculated data obtained by taking into consideration three low-energy conformers of (*R*)-EVD optimized at DFT level. The density functional theory (DFT)

1

employed for CD spectral simulations is a widely applied quantumchemical method to correlate chiroptical data with structural information.[5,6] The use of the Becke-Perdew (BP) functional basis set implemented in Turbomole program yielded the best agreement with the measured CD spectra.

Experimental Details

Materials

HSA (Sigma, A1887, 97%, essentially fatty acid-free), AAG (Sigma), (±)-evodiamine (Sigma), rutaecarpine (AK Scientific, Inc.), biliverdin HCl (Frontier Scientific), (±)-naproxen (AK Scientific, Inc.), (±)-flurbiprofen (Sigma), diazepam (Sigma), (*R*)- and (*S*)-oxazepam acetate,[7] and 5β-cholanic acid (Sigma) were used as supplied. HPLC grade ethanol (EtOH), trifluoroethanol (TFE), dimethyl sulfoxide (DMSO), acetonitrile (AcN), dioxan, and dichloromethane were used for spectroscopic measurements.

HSA binding test

Chromatographic experiments on HSA-Sepharose gel were performed as described previously.[7,8] EVD and RTC were detected at 280 nm and 344 nm, respectively. In control experiments performed on a gel containing no HSA, only RTC showed non-specific adsorption (elution volume was 9 mL on a V_0: 6 mL column).

Chiral HPLC analysis of EVD

The HPLC experiments were performed with a system composed of a JASCO PU-980 pump, a Rheodyne 7125 injector (20 μL loop), a JASCO MD 2010-Plus UV-Vis photodiode-array detector and Chrom Pass chromatographic software. CHIRALCEL® OJ column (250 × 4.6 mm i.d.) was obtained from Chiral Technologies Europe. The mobile phase was hexane/ethanol 60/40, flow rate was 0.9 mL/min. Detection was made at 225 nm. The elution order, *i.e.* first eluted (*S*)-(+) followed by (*R*)-(−)-enantiomer, was taken

from the work of Nguyen *et al.*[4] This method was used to prepare enantiomer samples for CD spectroscopic studies. In comparison with the chiroptical data reported for the (*S*)-(+)-EVD,[9] CD spectra of the samples confirm the assignment.

Ultrafiltrations were performed in the Amicon MPS-1 system, using YMT30 membranes. The enantiomeric composition of free EVD in the ultrafiltrates was determined by chiral HPLC method. Due to very high adsorption loss, ultrafiltration was not suitable for quantitative binding study.

Preparation of alkaloid and serum protein solutions

2 mM stock solution of EVD and RTC were prepared freshly before each measurement in DMSO or in dioxan. Water, water-DMSO, and buffer-DMSO mixtures were used to dissolve other compounds. The volume of DMSO added into protein solutions never exceeded 5% (v/v) and caused negligible effects either on the CD or the fluorescence spectra. HSA and AAG samples were dissolved in pH 7.4 Ringer buffer solution.

Circular dichroism and UV absorption spectroscopic measurements

CD and UV absorption spectra were recorded on a JASCO J-715 spectropolarimeter at 25 ± 0.2 °C. Temperature control was provided by a Peltier thermostat equipped with magnetic stirring. Alkaloid-serum protein CD titration experiments were performed in a rectangular quartz cell of 1 cm optical path length (Hellma, USA). Each spectrum represents the average of three scans obtained by collecting data at a scan speed of 100 nm/min. CD and UV spectra of (±)-EVD and its enantiomers were recorded in 0.2 cm and 1 cm rectangular quartz cells. Absorption spectra were obtained by conversion of the high voltage (HT) values of the photomultiplier tube of the CD equipment into

absorbance units. CD and absorption curves of alkaloid-serum protein mixtures, EVD enantiomers, and RTC were corrected by subtracting the spectra of alkaloid-free buffer solution of proteins and blank organic solvents. JASCO CD spectropolarimeters record CD data as ellipticity ('Θ') in units of millidegrees (mdeg). The quantity of 'Θ' is converted to '$\Delta\varepsilon$' values using the equation $\Delta\varepsilon = \Theta/(33982cl)$, where '$\Delta\varepsilon$' is the molar circular dichroic absorption coefficient expressed in $M^{-1}cm^{-1}$, 'c' is the molar concentration of the ligand (mol/L), and 'l' is the optical pathlength expressed in cm.

Calculation of HSA binding parameters of ($\pm$)-EVD and RTC from CD titration data

The association constant (K_a) was estimated using the following equation:[10]

$$CD(m\deg) = \frac{k}{2}\left(c_P + c_L + K_a^{-1} - \sqrt{\left(c_P + c_L + K_a^{-1}\right)^2 - 4c_Pc_L} \right)$$

'*CD*' is the induced ellipticity value of EVD and RTC measured at 355 and 343.2 nm at increasing alkaloid/HSA molar ratios, while 'c_L' and 'c_P' represent the total concentrations (in mol) of the alkaloids and HSA in the sample solution. 'k' is a constant defined by *CD*/[LP], where [LP] is the molar concentration of the alkaloid-HSA complexes. Non-linear regression analysis using Microcal Origin ver. 8.6 was performed to calculate the value of k and K_a.

Fluorescence spectroscopic measurements

Fluorescence measurements were carried out in a JASCO FP 8300 spectrofluorometer at 23 ± 1 °C, using a quartz cuvette with 1 cm optical path length, both bandwidths were 5 nm. Intensities were corrected for the inner filter effects according to the absorbance of the added alkaloids at both the excitation and emission wavelengths. The association

binding contants were calculated by the equation adapted from the work of Breusted et al.[11] assuming 1:1 stoichiometry, using non-linear regression analysis (Microcal Origin ver. 8.6).

Molecular modeling calculations

Docking calculations were carried out using DockingServer.[12] X-ray structures of HSA and the F1/S variant of AAG (PDB id. 2BXD, 3KQ0) were selected. All water molecules were removed from the protein coordinates prior to docking calculations. Hydrogen atoms were added to the PDB structure using AutoDockTools. The total charge of HSA and partial charges of the atoms were calculated by the Mozyme function of MOPAC2009 software. The calculated partial charges were applied for further calculations. Affinity (grid) maps of $30 \times 30 \times 30$ Å grid points were generated using the Autogrid program. AutoDock parameter set- and distance-dependent dielectric functions were used in the calculation of the van der Waals and the electrostatic terms, respectively. Docking simulations were performed using the Lamarckian genetic algorithm and the Solis & Wets local search method. PM6 semi-empirical method (MOPAC2009) was used for energy minimization and partial charges calculation for RTC. For (*R*)-EVD (neutral form), mirror image of the solid state structure of the (*S*)-enantiomer was used.[13] Initial position and orientation of the ligand molecules were set randomly. Each docking experiment was derived from 100 different runs that were set to terminate after a maximum of 2500000 energy evaluations. The population size was set to 150. During the search, a translational step of 0.2 Å, and quaternions and torsion steps of 5 were applied.

6

The outputs of docking calculations were rendered with PyMOL (The PyMOL Molecular
Graphics System, DeLano Scientific LLC, Palo Alto, CA, USA, http://www.pymol.org).
The conformational analysis of (*R*)-EVD was performed with the Conformer plugin
implemented in the Marvin 6.3.0 package using Dreiding force field (ChemAxon, Ldt.,
2014). The optimization limit was set in normal mode and the maximum number of
conformers was chosen for 20 with 0.1 diversity limit.

DFT (density functional theory) calculations

Theoretical CD spectrum calculation for three conformers of (*R*)-EVD in AcN was made
employing Turbomole v6.5 suite (COSMOlogic GmbH).[14,15] To consider the effect of the
solvent on the CD spectra of the individual conformers, the DFT optimization and the
rotatory strength calculations were performed at the BP/SVP DFT level of theory
combined with Conductor-like Screening Model (COSMO) as implemented in the
Turbomole program. The dielectric constant (ε) of 37.5 (AcN) and optimized atomic radii
(C: 2.00 Å, N: 1.83 Å, O: 1.72 Å, H: 1.30 Å) for the construction of the molecular cavity
were used for the calculation of each conformers. The applied DFT level includes the
following BP86 GGA (generalized gradient approximation) exchange-correlation
functional: exchange local density approximation (LDA) + Becke B(88), correlation
LDA (VWN) + Perdew (P86) combined with the SVP for both the atom-centered and the
auxiliary basis sets. The CD spectra were simulated by overlapping Gaussian functions
for each transition according to the equation:

$$\Delta\varepsilon\,(E) = \frac{1}{2.297 \times 10^{-39}} \frac{1}{\sqrt{2\pi\sigma}} \sum_{i}^{A} \Delta E_i\, R_i e^{[-(E - \frac{\Delta E_i}{2\sigma})]^{\mathrm{D}}}$$

8

where $\Delta\varepsilon$ is the molar dichroic absorption coefficient (M^{-1} cm^{-1}), σ is the width of the band at 1/e height (0.16 eV) and ΔE_i and R_i are the excitation energies and rotatory strengths for transition i, respectively.

Results

HSA binding study by affinity chromatography

Binding affinity of (±)-EVD and RTC to HSA was evaluated from their retentions on a HSA-Sepharose column, where the elution volume is characteristic of the binding affinity (nK_a).[7] Oxazepam acetate enantiomers and diazepam were used as reference compounds (Suppl. Table 1). (±)-EVD was eluted in two peaks (Fig. 1A) while RTC showed very high retention, revealing the stereoselective binding for EVD and very strong binding of RTC. Results in Suppl. Table 1 indicate binding constant values of about 1×10^5 M^{-1} and 2×10^5 M^{-1} for EVD enantiomers, while in case of RTC nK_a of $\sim 1 \times 10^6$ M^{-1} can be evaluated.

Characterization of binding stereoselectivity of (±)-EVD on HSA and AAG

Identification of enantiomers separated on the HSA-Sepharose column was performed by chiral HPLC analysis. The eluent fractions belonging to the two peaks were extracted by chloroform, and after vacuum evaporation of the solvent, the materials were dissolved in a small amount of ethanol. The elution order on the applied Chiralcel OJ column is known to be (*S*)-(+)- followed by (*R*)-(–)-EVD.[4] The samples obtained from the HSA column showed that the first peak refers to (*S*)-(+)-EVD and the more retained peak contains the (*R*)-enantiomer. The stereoselective binding of EVD on HSA and AAG was also studied by chiral HPLC analysis of the ultrafiltrates obtained from solutions containing the racemic ligand (20 μM) and the protein (30 μM). The injected samples were prepared as described above. Results showed (Fig. 1B) that (*S*)/(*R*) enantiomeric

ratios for the free ligand were 67/33 and 58/42 in HSA and AAG solutions, respectively. It is in accordance with the stereoselectivity value of $K_R/K_S \approx 2$ for HSA binding, obtained by affinity chromatography (Table 1). In the case of AAG, also the binding of the (R)-enantiomer is preferred, but the stereoselectivity is weaker. Similar experiments performed with the AAG F1-S and A genetic variants resulted in values of 60/40 and 53/47 for (S)/(R) enantiomeric free ligand ratios, respectively.

UV spectroscopic features of EVD and RTC

EVD consists of two, unconjugated indole and quinazolinone chromophoric units, the electronic transitions of which are superposed on each other in the absorption spectrum (Fig. 2). The indole ring gives rise to ^1L_b (~280 nm), ^1L_a (~270 nm), and a ^1B_b (~220 nm) type π-π^* band above 200 nm. The ^1L_b transition exhibits vibrational fine structure with two peaks between 280-300 nm being separated from each other by 1040 cm^{-1} in EVD (Fig. 2). The λ_{max} value of the ^1L_a transition is close to that of the ^1L_b so these bands considerably overlap with each other. Due to the small excitation energy difference, the analogous transitions of the quinazolinone moiety can not be distinguished in the spectrum. The major contributions to the most intense absorption peak of EVD between 223-228 nm come from the electronic dipole allowed π-π^* transitions of the aromatic chromophores. According to the second derivative analysis (not shown), this band consists of two unresolved peaks centered around 222 and 231 nm which can be assigned to the ^1B_b transition of the indole and the quinazolinone rings, respectively. The ^1B_b transition moment is polarized along the long axis of the indole ring[16] but no data available on the exact ^1B_b polarization direction of the quinazolinone moiety. In relation

10

to protic media, the λ_{max} value of the ^1B_b band is red shifted in apolar solvents (Fig. 2). The weak, long wavelength tail of EVD above 300 nm stems from electronically forbidden π-π^* transitions of the quinazolinone ring. The very weak n-π^* band of the amide group is buried under the π-π^* peaks below 300 nm.[17]

The presence of the double bond in the 'D' ring of RTC alters drastically the absorption spectrum. A new, intense band appears above 300 nm ($\varepsilon_{max} \approx 35,000$ M^{-1} cm^{-1}) showing a characteristic vibronic progression (Fig. 2). Distinctly from the L_b band of the indole ring, the 0$\rightarrow$0 and 0$\rightarrow$1 vibrational sub-bands are separated by a larger extent (1320 cm^{-1}). Showing a similar vibronic spacing (1270 cm^{-1}), a less intense absorption band ($\varepsilon_{max} \approx$ 3600 M^{-1} cm^{-1}) is displayed in the UV spectrum of 3-methyl-4-quinazolone between 280 and 330 nm which can be considered as the indole-free derivative of RTC.[18] Upon conjugation with the indole nucleus, this band is red shifted to 345 nm and exhibits a large intensity increase presumably due to the electron donating ability of the indole moiety (charge transfer).

Conformational and chiroptical properties of EVD

The indoloquinazolinone skeleton of EVD consists of an essentially planar indole (A and B), benzene (E), a non-planar cyclohexane (C) and pyrimidone ring (D) among which 'C' and 'D' are responsible for the conformational flexibility of the molecule (Scheme 1). Results of the conformational analysis of EVD show two additional low-energy species besides the solid state conformation (Fig. 3). In the latter case (L-shaped structure), the molecule is folded in the middle, about the line joining C7 and C13b atoms. The dihedral angle (φ) measured between the terminal phenyl groups is about 90°, the 'C' and 'D' ring

11

adopt a sofa conformation. In the other conformers, the value of φ increases resulting in a partially unfolded, ridge-tile (122°) and a fully unfolded, nearly flat geometry (176°) (Fig. 3) which are similar to those obtained for (*S*)-EVD by Pearce *et al.*[19]

According to their opposite absolute configurations, the chromatographically separated antipodes exhibit mirror-image CD curves (Suppl. Fig. 1). The CD pattern of (*R*)-EVD is substantially solvent dependent (Fig. 4). In water/dioxan mixture, EtOH and AcN a positive and a negative CD band can be seen above 300 nm associated to the long-wavelength tail of the absorption spectrum. Between 280 and 300 nm, a negative ellipticity peak appears bearing a vibrational fine structure which coincides with that of the corresponding UV band of the indole ring. In EtOH, CH_2Cl_2, and dioxan, a well resolved negative ellipticity band is displayed around 257 nm though no separate UV peak is allied to it. In dioxan and CH_2Cl_2, this band shows a suppressed vibrational progression which, however, lacks from the ethanolic spectrum. In aqueous solutions and AcN, this peak is blue shifted below 254 nm and it can be observed as a shoulder only. Allied to the ^1B_b UV band of the indole and quinazolinone chromophore, a negative-positive CD couplet is displayed in AcN and water/dioxan mixture, with extrema at about 231-233 and 220 nm (Suppl. Fig. 1, Fig. 4). The zero-crossover point between these opposite peaks at 224 nm is close to the UV maximum. In dioxan, CH_2Cl_2, and Ringer buffer, only the negative branch of the couplet is displayed due to the UV cut-off wavelength of the solvents. The intensity ratio of the CD bands at 257 and 231-233 nm largely increases in less polar (EtOH) and apolar solvents (dioxan, CH_2Cl_2).

DFT calculations[20,21] performed on the L-shaped conformer of (*R*)-EVD in AcN showed a negative-positive CD band pair below 245 nm (Fig. 5A). This spectral pattern bears a

close resemblance to the high-energy part of the experimental CD curve obtained in polar solvents (AcN, water/dioxan, EtOH). In contrast, this CD couplet is absent from the spectrum predicted for the flat conformer (Fig. 5A). The calculated CD curve of the L-shaped conformer above 280 nm exhibits a lower-wavelength negative and a higher-wavelength positive band (Fig. 5A) in good agreement with that measured in AcN, water/dioxan mixture, and buffer solution (*cf.* Fig. 4). In the same wavelength range, the simulated CD profile of the ridge-tile structure of (*R*)-EVD (Fig. 5B) is similar to the ICD curve of (±)-EVD-HSA and (*R*)-EVD-HSA complexes (*vide infra*).

Plasma protein binding induced CD and absorption spectroscopic changes of (±)-EVD and its enantiomers

The absorption bands of (±)-EVD above 250 nm were rendered optically active upon association with HSA giving rise to positive CD peaks of distinct magnitudes around 266 nm and 357 nm (Fig. 6). This induced CD (ICD) pattern remained invariant upon raising the [L]/[P] ratio. Due to the strong masking effect of the intrinsic CD and UV activity of HSA, the CD spectrum of EVD cannot be recorded below 250 nm. The apparent HSA association constant ($K_a = 1.4 \times 10^5$ M^{-1}) calculated from the ellipticity changes (Suppl. Fig. 2) is in accordance with the affinity chromatography result. In comparison to the low-intensity tail recorded in protein-free buffer solution, the absorbance values of EVD above 320 nm are more intense and a well-resolved band is shown centered around 356 nm (Suppl. Fig. 2). In HSA bound state, the CD spectra of (*R*)- and (±)-EVD are similar to each other (Fig. 7A). HSA binding renders the ellipticity values of (*S*)-EVD more intense and the positive CD band displayed around 250 nm in buffer solution is red

13

shifted by about 7 nm (Fig. 7B). Importantly, arithmetic sum of the CD curves of (*R*)- and (*S*)-EVD measured in HSA solution completely matches with the CD spectrum of the racemic sample obtained under the same conditions (Fig. 7A).

The UV spectrum of (±)-EVD measured with the main genetic variants of AAG is similar to that found with HSA. In relation to the A form, a better resolved vibrational fine structure and less intense band above 300 nm could be seen in the absorption spectrum of (±)-EVD measured with the F1/S variant (Suppl. Fig. 3). A more salient difference was observed between the chiroptical responses: while the A variant was not able to generate any difference CD activity for (±)-EVD, an ICD curve similar to that measured with HSA was obtained with the F1/S form (Suppl. Fig. 3). Distinctly from the shorter-wavelength ellipticity peak of the albumin-bound alkaloid, CD band of the EVD-F1/S complexes exhibits two, partially resolved sub-bands at 260 and 280 nm, respectively. Nevertheless, these low-intensity ICD values did not allow quantitative evaluation of the EVD binding to AAG.

Study of (±)-EVD binding to HSA and AAG by fluorescence spectroscopy

The effect of EVD on the intrinsic fluorescence of HSA can be seen in Fig. 8. Excitation was made at 295 nm, thus the emission at 338 nm represents the single Trp214 in subdomain IIA of the protein. Results proved that EVD not only quenched the intrinsic Trp fluorescence, but an emission peak developed at 424 nm, belonging to the bound EVD. There is an isoemission point at 393 nm and the two bands partially overlap with each other. In relation to the emission peak of the bound species, fluorescence of the free EVD is very weak and red shifted. By using an excitation wavelength of 360 nm, only the

emission of the bound EVD could be detected. Based on the emission data recorded at 424 nm, association binding constant of 1.8×10^5 M^{-1} could be calculated, which is in good agreement with the results evaluated by HSA affinity chromatography and CD spectroscopic studies (Table 1). In order to identify the specific albumin binding site of EVD, fluorescence displacement measurements were carried out by applying some non-fluorescent drugs which are known to bind specifically to the principal binding sites of albumin. In the presence of diazepam and (±)-flurbiprofen, which are high-affinity marker ligands of site IIIA,[22] no significant intensity changes could be observed (data not shown).

The binding of EVD to AAG showed similar fluorescence behaviour (Fig. 8). There is a quenching of protein fluorescence at 335 nm and simultaneous development of an emission peak at 428 nm indicating the bound EVD. In comparison to HSA, the two bands are better separated. The emission spectrum of AAG reflects the contribution of three Trp residues, two of them residing inside the central hydrophobic cavity, while the third residue is located on the outer surface exposed to solvent.[23] The estimated affinity constant (9.8×10^5 M^{-1}) reveals about five times stronger EVD-AAG binding interaction compared to HSA (Table 1). Similar experiments performed with the F1/S and A genetic variants resulted in K_a values of 1.9×10^6 and 8.3×10^5 M^{-1}, respectively. The displacing effect of EVD on ANS-AAG complexes was studied, too. ANS is a specific fluorescent label which is known to bind in the hydrophobic cavity of AAG.[11] The excitation was made at 420 nm, when EVD shows no emission (Suppl. Fig. 4). The displacing ability of EVD was found to be only slightly weaker compared to that of chlorpromazine, a high-

affinity ligand ($K_a \approx 2 \times 10^6$ M^{-1}) of AAG.[24,25] This finding confirms the strong binding of EVD within the cavity of AAG.

Identification of the HSA binding site of EVD by CD displacement method

To locate the EVD binding site on HSA, molecular probes can be used which are specific to the main drug binding regions of the protein situated in subdomain IB, IIA, and IIIA, respectively. Accomodation of biliverdin at site IB induces an intense, positive CD peak between 330 and 440 nm which gradually decreases upon addition of competing ligands bound here.[26] Some site IIA and IIIA ligands, however, often increase the ICD band of biliverdin through allosteric mechanism.[26] Similarly to these agents, substantial intensity enhancement was measured upon addition of ($\pm$)-EVD to biliverdin-HSA mixture (Suppl. Fig. 5). Naproxen is the high-affinity marker of site IIIA ($K_a \sim 10^6$ M^{-1}) but it displays no CD activity upon HSA association.[27] Raising the concentration of this drug in the sample solution did not affect the ICD curve of EVD (data not shown). Site IIIA also hosts 5β-cholanic acid[28] that significantly increased the ellipticity values of the HSA-bound EVD and blue shifted the λ_{max} of the low-energy CD peak by about 18 nm (Suppl. Fig. 6). The third principal binding area is located in the large cavity of subdomain IIA consisting of several sub-sites.[29] Since this pocket can simultaneously engulf two ligand molecules,[29,30] it is worth to use a bulky marker compound which prevents the co-binding of EVD. For this purpose, chenodeoxycholic acid was selected which inhibits the binding the subdomain IIA marker warfarin to HSA.[31] Its addition reduced the amplitude of the ICD band of EVD by about 60% and also rendered the UV band of the alkaloid similar to that

16

measured in buffer solution (Suppl. Fig. 7). The fluorescence quenching of Trp214 of HSA also supports the subdomain IIA binding of EVD (Fig. 8).

CD spectroscopic manifestations of RTC-HSA and RTC-AAG interactions

Upon sequential addition of RTC into HSA solution, a monophasic ICD pattern evolved displaying two, broad negative bands above and below 290 nm (Fig. 9). The position and vibrational structure of the long-wavelength peak closely match with the corresponding absorption band centered at 342 nm. However, no resolved UV peak is allied to the ellipticity band around 260 nm. In relation to the free form, the absorption maximum of RTC is red shifted by 6 nm in the presence of HSA. Above the [RTC]/[HSA] ratio of 0.6, however, the ICD curve becomes polyphasic showing a positive peak at 370 nm of which amplitude proportionally raises with the concentration of RTC (Fig. 9). Two additional negative peaks also appear, a weaker one at 360 nm and a more intense at 344 nm. At the same time, the CD signals below 335 nm remain invariant showing neither qualitative nor quantitative changes (Suppl. Fig. 8). The affinity constant estimated from the ICD data measured at 343 nm is higher by an order of magnitude than that obtained for EVD-HSA binding (Table 1). Displacement studies could not be performed with RTC since its free fraction forms aggregates in aqueous solution resulting artefacts in the CD spectra.

By contrast to HSA, the AAG induced ellipticity signals of RTC are weak and noisy (not shown) hampering reliable estimation of the binding constant from the CD data.

Study of RTC binding to HSA and AAG by fluorescence spectroscopy

Addition of RTC to HSA and AAG solutions produced similar changes shown with EVD.

RTC also effectively quenched the intrinsic protein fluorescence and emission of bound RTC appeared at about 400 nm. Unfortunately, the fluorescence of free RTC was found to be unstable, its intensity enhanced by time, disturbing quantitative evaluations. Nevertheless, the binding constant could be evaluated by using high protein concentration (20 μM) and excitation wavelength of 360 nm. Emission spectra of free and bound RTC are displayed in Suppl. Fig. 9. Based on emission values at 400 nm, binding constant values of 1.3×10^6 M^{-1} and 4.3×10^6 M^{-1} could be determined for HSA and AAG, respectively. This tight HSA binding is in accordance with the results obtained by affinity chromatography and CD studies.

Targeted molecular docking of (R)-EVD and RTC to subdomain IIA of HSA

In view of the displacement results, (*R*)-EVD was docked into the pocket of subdomain IIA of HSA. Conformational adjustment of the crystallographic structure of the molecule[13] was allowed during the docking procedure. According to the best energy result, EVD is buried within the hydrophobic pocket where it adopts ridge-tile conformation (Fig. 10) and establishes hydrophobic contacts with Trp214 and aliphatic side chains (Ala215, Leu219, Leu238, Ile264, Ile290, Ala291). The indole nitrogen and carbonyl oxygen atom of EVD form H-bond with Arg222 and Tyr150, respectively. Similar docking studies were performed with RTC. Distinctly from EVD, the quinazolinone part of RTC forms π-π stacking interaction with Trp214 (3.3 Å) and there is an H-bond between the indole nitrogen and the Asp451 side chain (Fig. 10).

18

Discussion

EVD is a chiral molecule with an asymmetric centre at the C3 position. Samples of natural origin are supposed to contain the (*S*)-(+)-enantiomer while the synthetic drug is a racemic mixture. In fact, analysis of 13 commercial *Evodiae fructus* samples by a recently developed chiral HPLC method indicated the presence of 6-25% (*R*)-(–)-EVD, the amount of which was increased due to heating. On the other hand, in the extract of the root bark of *Zanthoxylum budrunga* the racemic form was identified.[32] There are only a few reports related to the link between the chirality and pharmacological effects of EVD. In an *in vitro* antiproliferative assay, performed with H460 cells, (*S*)-EVD was found to be about five times more potent compared to its enantiomer.[33] In that test, however, the (*R,R*)-enantiomer of a 5-substituted analogue showed preference of similar extent compared to the (*S,S*)-form. It has also been shown that the vanilloid receptor activity of (*S*)-EVD is more efficacious and potent than the (*R*)-enantiomer.[34] We found that a chiral discrimination exists in the HSA binding of EVD both in quantitative and qualitative sense. The affinity of (*R*)-EVD to HSA is about twice compared to the (*S*)-enantiomer (Fig. 1, Table 1). Moreover, the CD spectroscopic results proved that the enantiomers have even different binding modes. While the CD spectra of the bound and free (*S*)-EVD show limited differences, gross spectral changes for the (*R*)-enantiomer were induced (Fig. 7B) suggesting that a substantially altered conformation is preferred at the binding site in relation to its free form. Comparison of the calculated and ICD spectra of (*R*)-EVD indicates the prevalence of the folded (L-shaped) conformer in polar (aqueous) solution (Fig. 5A) and that of the partly unfolded (ridge-tile) species at the hydrophobic HSA

binding site (Fig. 5B). In contrast, moderate alteration of the CD pattern of the (*S*)-enantiomer upon HSA association refers to slight conformational changes only, which may be the structural basis of the observed enantioselectivity.

Although EVD associates to AAG ten-times stronger than to HSA (Table 1), the large abundance of the latter in plasma (600 μM HSA *vs*. 15-30 μM AAG) suggests that in healthy subjects albumin binding determines the pharmacologically active free serum level of EVD. Under various pathological conditions, however, when the concentration of AAG increases by 3-4 times, the unbound fraction of EVD might be significantly reduced.[35] According to the results, the free serum fraction of racemic EVD is likely featured with the relative dominance of the (*S*)-enantiomer. From a practical point of view, the above findings also imply that HSA is a promising agent for separation of stereoisomers of EVD and related compounds.

Interestingly, there is a significant difference between the enantioselectivities of the genetic variants of AAG.[36] Similarly to that found with HSA, the F1/S form prefers the (*R*)-enantiomer, while the enantiodiscrimination of the A variant is almost negligible (Table 1). These findings help to understand the distinct CD spectroscopic behaviour of (±)-EVD obtained with the AAG variants (Suppl. Fig. 3). Distinctly from the F1/S form, EVD enantiomers bind to the A variant approximately in the same extent so their chiroptical contributions mutually cancel each other resulting no ICD activity (assuming their similar binding modes).

Fluorescence quenching (Fig. 8) and CD displacement data (Suppl. Fig. 7) indicate that EVD is accomodated in the large drug binding cavity of subdomain IIA, near to the sole Trp214 residue of the protein. As it can be inferred from the CD spectroscopic changes,

20

this binding region of EVD is allosterically coupled with the other principal ligand

binding pockets of HSA. Entrapment of the EVD molecule within subdomain IIA

enhances the selectivity of the site IB pocket in favour to the *M*-helical form of biliverdin

(Suppl. Fig. 5).[26] Furthermore, inclusion of 5β-cholanic acid into subdomain IIIA affects

the binding interaction of EVD at site IIA (Suppl. Fig. 6).

As it is suggested by the CD spectra, EVD can adopt different conformations depending

on the polarity and H-bonding properties of its environment (Fig. 4). The intense CEs of

opposite sign measured below 245 are associated to the strong UV peak of EVD. It is a

typical situation for exciton coupling that occurs intramolecularly between the π-π^*

transitions of the indole and quinazolinone moiety. Taking into consideration the first

negative and the second positive exciton CE of (*R*)-EVD, the exciton chirality method[37,38]

predicts that the interacting ^1B_b dipole moments form a left-handed screwness (negative

chirality). According to the angular dependence rule,[39] exciton band intensities are

maximal when the dihedral angle between the planes of the interacting chromophores is

around 70º. That angle in the folded, L-shaped conformation of EVD (~90º) is close to

this value (Fig. 3) suggesting the dominant contribution of the same or a very similar

conformer in polar solvents. This assumption is supported by quantum chemical

calculation of the CD spectrum of the L-shaped EVD reproducing not only the high-

energy exciton couplet but also the ellipticity pattern in the near-UV region (Fig. 5A). In

apolar medium, the conformational equilibrium of EVD seems to be shifted toward

unfolded, flattened structures causing intensity loss of the exciton CEs (Fig. 4) that is

consistent with the lack of exciton signals from the calculated CD spectrum of the flat

conformer of EVD (Fig. 5A).

Taking into consideration the characteristic blue shift seen in polar solvents, the n-π^* transition of the amide group of EVD can be assigned to the negative CE measured between 245 and 270 nm (Fig. 4). Sign and intensity of this band is determined by the mutual contribution of the chiral first and second sphere around the amide chromophore.[40] The folded→unfolded shift of EVD is accompanied by the intensity increase of this band also indicating steric changes of the molecule.

Distinctly from EVD, RTC binds to both HSA and AAG with much higher affinity (Table 1). Enhanced hydrophobicity and the altered geometry of the indolopyridoquinazolinone ring system might be responsible for its tighter protein association. The rigid, planar structure of RTC is favourable for a π-π stacking with aromatic residues of the binding environment (Fig. 10). The spatial proximity of the Trp214 side chain of HSA to the alkaloid molecule bound at site IIA and the consequent non-degenerate exciton coupling between them is the possible source of the induced ellipticity bands observed in the CD spectrum of RTC at low L/P ratios (Fig. 9). The large binding room of subdomain IIA and the planar geometry of RTC, however, can mutually facilitate the insertion of a second ligand molecule into the pocket resulting in positive-negative CD signals (Fig. 9) which are indicative to a degenerate, ligand-ligand exciton coupling interaction.[41]

Conclusions

The results presented herein show that EVD possesses structural flexibility represented by conformational transitions between folded and unfolded forms of the molecule. This inherent stereochemical feature is important to understand structure-activity relationships and the molecular basis of the manifold pharmacological activities of EVD. Comparative evaluation of the experimental and calculated CD data enabled (i) to assign the predominant conformation of EVD in polar media, (ii) to recognize intramolecular exciton coupling in the folded (L-shaped) conformer of the molecule, (iii) to correlate various conformational states of EVD with solvent dependent CD spectral changes, and (iv) to propose the preferred conformation of (R)-EVD at its HSA binding site. Allosteric HSA binding interactions as well as the enantioselective plasma protein association of EVD are also demonstrated showing the binding preference of the (R)-enantiomer both to albumin and AAG. The significantly tighter HSA association of RTC, as well as its dimeric HSA binding mode can be ascribed to its rigid, planar geometry which allows a large number of hydrophobic binding contacts and the snug fitting of two alkaloid molecules into the main chamber of site IIA.

23

Supporting Information

Additional experimental CD spectra and fluorescence titration data of EVD and RTC.

This material is available free of charge via the Internet at http://pubs.rsc.org.

Acknowledgements

References

1.   S. H. Lee, J. K. Son, B. S. Jeong, T. C. Jeong, H. W. Chang, E. S. Lee and Y. Jahng, *Molecules*, 2008, **13**, 272-300.

2.   H. Yu, H. Jin, W. Gong, Z. Wang and H. Liang, *Molecules*, 2013, **18**, 1826-1843.

3.   J. Jiang and C. Hu, *Molecules*, 2009, **14**, 1852-1859.

4.   N. V. Nguyen, K. R. Lee, Y. J. Lee, S. Choi, J. S. Kang, W. Mar and K. H. Kim, *J. Pharm. Biomed. Anal.*, 2013, **81-82**, 151-159.

5.   M. Orio, D. A. Pantazis and F. Neese, *Photosynth. Res.*, 2009, **102**, 443-453.

6.   J. Autschbach, T. Ziegler, S. J. A. van Gisbergen and E. J. Baerends, *J. Chem. Phys.*, 2002, **116**, 6930-6940.

7.   I. Fitos, Z. Tegyey, M. Simonyi, I. Sjöholm, T. Larsson and C. Lagercrantz, *Biochem. Pharmacol.*, 1986, **35**, 263-269.

8.   F. Zsila, J. Visy, G. Mády and I. Fitos, *Bioorg. Med. Chem.*, 2008, **16**, 3759-3772.

9.   B. Danieli, G. Lesma and G. Palmisano, *J. Chem. Soc.*, 1982, 1092-1093.

10.   F. Zsila, Z. Bikadi and M. Simonyi, *Biochem. Pharmacol.*, 2003, **65**, 447-456.

11.   D. A. Breustedt, D. L. Schonfeld and A. Skerra, *Biochim. Biophys. Acta*, 2006, **1764**, 161-173.

12.   Z. Bikadi and E. Hazai, *J. Cheminform.*, 2009, **1**, 15.

13.   I. Fujii, Y. Kobayashi and N. Hirayama, *Z. Kristallogr.*, 2000, **215**, 762-765.

14.   C. Diedrich and S. Grimme, *J. Phys. Chem. A*, 2003, **107**, 2524-2539.

15.	A. E. Nugroho and H. Morita, *J. Nat. Med.*, 2014, **68**, 1-10.

16.	B. Albinsson and B. Nordén, *J. Phys. Chem.*, 1992, **96**, 6204-6212.

17.	J. Heldt, J. R. Heldt and E. Szatan, *J. Photochem. Photobiol. A*, 1999, **121**, 91-97.

18.	J. M. Hearn, R. A. Morton and J. C. E. Simpson, *J. Chem. Soc.*, 1951, 3318-3329.

19.	L. V. Pearce, P. A. Petukhov, T. Szabo, N. Kedei, F. Bizik, A. P. Kozikowski and P. M. Blumberg, *Org. Biomol. Chem.*, 2004, **2**, 2281-2286.

20.	S. Ionescu, I. Matei, C. Tablet and M. Hillebrand, *Phys. Chem. Chem. Phys.*, 2013, **15**, 11604-11614.

21.	R. Sandu, C. Tablet and M. Hillebrand, *J. Incl. Phenom. Macrocycl. Chem.*, 2013, **77**, 183-193.

22.	I. Sjöholm, B. Ekman, A. Kober, I. Ljungstedt-Pahlman, B. Seiving and T. Sjödin, *Mol. Pharmacol.*, 1979, **16**, 767-777.

23.	D. L. Schönfeld, R. B. Ravelli, U. Mueller and A. Skerra, *J. Mol. Biol.*, 2008, **384**, 393-405.

24.	F. Hervé, G. Caron, J. C. Duché, P. Gaillard, N. Abd Rahman, A. Tsantili-Kakoulidou, P. A. Carrupt, P. d'Athis, J. P. Tillement and B. Testa, *Mol. Pharmacol.*, 1998, **54**, 129-138.

25.	I. Fitos, J. Visy, M. Simonyi, G. Mády and F. Zsila, *Biochim. Biophys. Acta*, 2010, **1800**, 367-372.

26.	F. Zsila, *Mol. Pharm.*, 2013, **10**, 1668-1682.

27.	C. Bertucci, *Chirality*, 2001, **13**, 372-378.

26

28. F. Zsila, *J. Phys. Chem. B*, 2013, **117**, 10798-10806.

29. J. Ghuman, P. A. Zunszain, I. Petitpas, A. A. Bhattacharya, M. Otagiri and S. Curry, *J. Mol. Biol.*, 2005, **353**, 38-52.

30. L. Zhu, F. Yang, L. Chen, E. J. Meehan and M. Huang, *J Struct Biol*, 2008, **162**, 40-49.

31. C. J. Bowmer, P. G. Donoghue, C. F. Leong and M. S. Yates, *J. Pharm. Pharmacol.*, 1985, **37**, 812-815.

32. B. S. Joshi, K. M. Moore, S. W. Pelletier and M. S. Puar, *Phytochem. Anal.*, 1991, **2**, 20-25.

33. M. S. Christodoulou, A. Sacchetti, V. Ronchetti, S. Caufin, A. Silvani, G. Lesma, G. Fontana, F. Minicone, B. Riva, M. Ventura, M. Lahtela-Kakkonen, E. Jarho, V. Zuco, F. Zunino, N. Martinet, F. Dapiaggi, S. Pieraccini, M. Sironi, L. Dalla Via, O. M. Gia and D. Passarella, *Bioorg. Med. Chem.*, 2013, **21**, 6920-6928.

34. L. De Petrocellis, A. Schiano Moriello, G. Fontana, A. Sacchetti, D. Passarella, G. Appendino and V. Di Marzo, *Br. J. Pharmacol.*, 2014, **171**, 2608-2620.

35. J. M. Kremer, J. Wilting and L. H. Janssen, *Pharmacol. Rev.*, 1988, **40**, 1-47.

36. E. Hazai, J. Visy, I. Fitos, Z. Bikádi and M. Simonyi, *Bioorg. Med. Chem.*, 2006, **14**, 1959-1965.

37. N. Berova, L. Di Bari and G. Pescitelli, *Chem. Soc. Rev.*, 2007, **36**, 914-931.

38. J. Grajewski, K. Gawronska and J. Gawronski, *Monatsh. Chem.*, 2005, **136**, 447-459.

39. N. Harada, S.-M. L. Chen and K. Nakanishi, *J. Am. Chem. Soc.*, 1975, **97**, 5345-5352.

40. G. Snatzke, *Angew. Chem. Int. Ed.*, 1979, **18**, 363-377.

41.   F. Zsila, Z. Bikádi and M. Simonyi, *Tetrahedron: Asymmetry*, 2001, **12**, 3125-3137.

	HSA	native	F1/S	A	Method
			AAG		
EVD	(S) 1.0×10^5	–	–	–	Aff. Chrom.
	(R) 2.0×10^5				Aff. Chrom.
	(±) $1.8(\pm0.4) \times 10^5$	$9.8(\pm0.6) \times 10^5$	$1.9(\pm0.16) \times 10^6$	$8.3(\pm1.1) \times 10^5$	Fluoresc.
	(±) $1.0(\pm0.2) \times 10^5$	–	–	–	CD
RTC	1.0×10^6	–	–	–	Aff. Chrom.
	$1.2(\pm0.2) \times 10^6$	$2.1(\pm0.4) \times 10^6$	$1.6(\pm0.3) \times 10^6$	$2.4(\pm0.3) \times 10^6$	Fluoresc.
	$1.4(\pm0.3) \times 10^6$	–	–	–	CD

Table 1

Plasma protein binding association constants (K_a in M^{-1}) of EVD and RTC evaluated by various methods.